Understanding the compaction behaviour of Low-substituted HPC: Macro, micro and nano-metric evaluations

Authors: Amr ElShaer[1,*], Ali Al-khattawi[2], Afzal R. Mohammed[2], Monika Warzecha[3] , Dimitrios A. Lamprou[3,4] , Hany Hassanin[5]

[1]Drug Discovery, Delivery and Patient Care (DDDPC), School of Life Sciences, Pharmacy and Chemistry, Kingston University London, Kingston-upon-Thames, Surrey, KT1 2EE, UK

[2]Aston Pharmacy School, Aston University, Aston Triangle, Birmingham B4 7ET, UK

[3]Strathclyde Institute of Pharmacy and Biomedical Sciences (SIPBS), University of Strathclyde, 161 Cathedral Street, Glasgow, G4 0RE, U.K.

[4]EPSRC Centre for Innovative Manufacturing in Continuous Manufacturing and Crystallisation, University of Strathclyde, Technology and Innovation Centre, 99 George Street, Glasgow, G1 1RD, U.K.

[5]School of Mechanical and Automotive Engineering, Kingston University London, Kingston Upon Thames, Surrey, KT1 2EE, UK

*** Corresponding author**

Dr Amr ElShaer

Drug Discovery, Delivery and Patient Care (DDDPC)

School of Life Sciences, Pharmacy and Chemistry Kingston University London

Penrhyn Road, Kingston-upon-Thames,

Surrey, KT1 2EE, UK

Email: a.elshaer@kingston.ac.uk

T +44 (0)20 8417 7416 (Internal: 67416)

Abstract

The fast development in materials science has resulted in the emergence of new pharmaceutical materials with superior physical and mechanical properties. Low-substituted hydroxypropyl cellulose is an ether derivative of cellulose and is praised for its multi-functionality as a binder, disintegrant, film coating agent and as a suitable material for medical dressings. Nevertheless, very little is known about the compaction behaviour of this polymer. The aim of the current study was to evaluate the compaction and disintegration behaviour of four grades of L-HPC namely; LH32, LH21, LH11 and LHB1. The macrometric properties of the four powders were studied and the compaction behaviour was evaluated using the out-of-die method. LH11 and LH22 showed poor flow properties as the powders were dominated by fibrous particles with high aspect ratios, which reduced the powder flow. LH32 showed a weak compressibility profile and demonstrated a large elastic region, making it harder for this polymer to deform plastically. These findings are supported by AFM which revealed the high roughness of LH32 powder (100.09±18.84 nm), resulting in small area of contact, but promoting mechanical interlocking. On the contrary, LH21 and LH11 powders had smooth surfaces which enabled larger contact area and higher adhesion forces of 21.01±11.35 nN and 9.50±5.78 nN respectively. This promoted bond formation during compression as LH21 and LH11 powders had low strength yield.

Keywords: L-HPC, Compaction, porosity, AFM, BET, disintegration time.

List of abbreviations

AFM	Atomic force microscopy
BET	Brunauer-Emmett-Teller
BJH	Barrett–Joyner–Halenda
ε	porosity
D_p	poured density
D_t	tapped density
L-HPC	low-hydroxypropyl cellulose
g	gram
LH-11	low-hydroxypropyl cellulose grade 11
LH-21	low-hydroxypropyl cellulose grade 21
LH-32	low-hydroxypropyl cellulose grade 32
LH-B1	low-hydroxypropyl cellulose grade B1
LH-41	low-hydroxypropyl cellulose grade 41
SEM	scanning electron microscopy
MCC	Microcrystalline cellulose
MP	micropore

ρ_d	bulk density
ρ_t	true density
VMD	volume mean diameter
s	second
XRD	X-ray powder diffractometry

1. Introduction

New pharmaceutical formulations continually emerge over the years, thanks to the fast development of materials science and the introduction of new pharmaceutical excipients. Understanding the physical and mechanical behaviour of pharmaceutical materials by evaluating their micro and macrometrics will help in developing successful delivery systems. Some of the pharmaceutical materials are of bio-based origin such as alginate, chitin-chitosan, poly lactic acid and cellulose. Cellulose is a widely used excipient in tablet manufacturing, the bio-based material was first isolated by a French Chemist in 1839 from plant matter (Purves., 1946). Nowadays, between 10^{10}-10^{11} tonnes of cellulose are produced annually to be used in chemical, material and textile industries (Azizi Samir et al., 2005).

As a bio-based material, cellulose offers unique characteristics such as good biocompatibility, high tensile strength, thermal stability and superior mechanical properties. Nonetheless, cellulose is poorly soluble in most of the common solvents and lacks the thermoplastic properties desired. Chemical and physical modifications of cellulose structure have been investigated (Roy et al., 2009; Hebeish and Guthrie, 1981), primarily via esterification reactions with nitrate and acetic acid derivatives (Klemm et al., 2005) and etherification with methyl, carboxy methyl and hydroxyalkyl derivatives (Fox et al., 2011).

Low-substituted hydroxypropyl cellulose is an ether derivative of cellulose, where a low percentage of hydroxyl groups (between 0.1 to 0.5%) in the repeating glucose units have been 'hydroxypropylated', forming $–OCH_2CH(OH)CH_3$ groups (Figure 1), using propylene oxide (Onda et al., 1978). Unlike typical HPC polymers (with 2- 4.5% substitution per glucose unit), L-HPC is water insoluble and commonly used as a binder and disintegrant in solid dosage forms (Shirai et al., 1994). L-HPC is praised for its multi-functionality. Not only it can be used as binder, but also, due to its inert nature, as a film coating agent for preparing floating systems (Diós et al., 2015) and in the preparation of medical dressings (Ogawa et al., 2014). Besides, L-HPC has been used to improve drug dissolution and oral bioavailability by forming dispersion systems with water insoluble drugs (Torre-Iglesias et al., 2014).

Sustained drug release is a common application of L-HPC as it forms a gel-layer around the tablet which then acts as a diffusion barrier. The water mobility and diffusion across L-HPC was evaluated in a study using magnetic resonance imaging (MRI) (Kojima and Nakagami., 2002). The study confirmed the formation of a gel-layer around the hydrated L-HPC tablet across which water mobility diminished, suggesting a restricted diffusion of water in all the hydrated tablets. In addition, LH41 was used in a series of studies by Kawashima et al (Kawashima et al., 1993)to control the release of acetaminophen. The study documented that LH41 managed to prolong the acetaminophen release at acidic pH for concentrations above 20%. On the other hand, substituting LH41 with coarse L-HPCs such as LH21, LH31 and LH11 resulted in tablets with immediate drug release because of the fast disintegration behaviour of these polymers. The discrepancies in the drug release behaviour among the four polymers were attributed to low water uptake for LH41 tablets, in addition to the formation of a continuous gel-layer across LH41 hydrated tablets (Kawashima et al., 1993).

The use of L-HPC as a disintegrant was also evaluated in the literature (Ishikawa et al 2001; Sunada and Bi 2002) and it is believed that L-HPC operates by a swelling disintegration mechanism due to water gathering around the substituted hydroxypropyl ($CH_2CH(CH_3)OH$) groups, increasing the L-HPC molecular size. Ishikawa and co-workers looked at formulating orally disintegrating tablets (ODTs) using mixtures of L-HPC and MCC at different ratios. It was found that tablets prepared from a mixture of MCC and L-HPC at a ratio of 9:1, had greater mechanical strength as well as fast disintegration times. When the compression force of 1-6kN was applied, the ODTs were able to withstand more than 3kg, indicating high hardness, but at the same time, underwent complete disintegration in 15 sec. It is important to note that the amount of L-HPC used influenced the rate of disintegration. Nevertheless, it was observed that by increasing the concentration of L-HPC to 40-50% in the mixture, the disintegration time became longer. Though the extent of swelling action mentioned above, which is utilised by the polymer is up 10 fold when compared to MCC, such a high amount starts to disrupt the wetting ability required for disintegration. Usually by increasing the concentration of L-HPC, the disintegration time decreased (Ishikawa et al., 2001).

Another study conducted by Sunada and Bi exhibited similar findings; the study attempted to formulate ODTs using a mixture of MCC and L-HPC using direct compression and wet compression. Wet granules were prepared and compressed at low compression forces prior to drying in circulating air oven. It was observed that mechanical strength increased when the proportion of MCC to L-HPC in the mixture increased. However, such mixtures also had reduced porosity. ODT containing a ratio of 7:3 MCC :L-HPC was tested, and found to have tensile strength and porosity of 3 MPa and 0.08, respectively. Whereas a 9:1 mixture had tensile strength and porosity of 3.6 MPa and 0.06,

respectively. It was observed that increasing tablets' tensile strength was associated with a drop in porosity and this was attributed to the ability of MCC to form a greater number of interactions using the hydroxyl groups in its structure when it underwent direct compression (Sunada and Bi 2002).
The Ishikawa et al and Sunada and Bi studies demonstrated that L-HPC can achieve success in manufacturing orally disintegrating tablets, maintaining the mechanical properties without sacrificing a fast disintegration time.

Despite the fact that many polymers have been studied in the field of ODTs, L-HPC is one polymer which has not been studied as extensively when compared to some of the polymers mentioned above. The potential of L-HPC in ODTs has been claimed by its manufacturers. However, a survey of the literature shows that very little is known about this polymer. Therefore, the focus of this study was to evaluate the compaction and disintegrating behaviour of four L-HPC grades namely LH21, LH32, LH11 and LHB1 (Table 1) during ODT manufacture. The nano, micro and macrometric properties of the four polymers were evaluated in order to understand their compaction mechanism.

Table 1: Summary of the properties of the four grades of L-HPC; LH31, LHB1, LH21 and LH11 reported by the manufacturer (Shin-Etsu).

L-HPC grade	Average molecular weight	Hydroxypropyl content %	Degree of polymerisation	Characteristics
LH32	115,000	8	660	White, fine powder
LHB1	140,000	11	790	White, coarse powder
LH21	120,000	11	680	White, coarse powder
LH11	130,000	11	730	White, coarse powder

2. Materials and methods

2.1. Materials

Low-substituted hydroxypropylcellulose grade LH21, Low-substituted hydroxypropylcellulose grade LHB1, Low-substituted hydroxypropylcellulose grade LH11, Low-substituted hydroxypropylcellulose grade LH32 all were gifted from Shin-Etsu Chemical Co. Ltd.(Chiyoda-Ku, Tokyo, Japan).

2.2. Methods

2.2.1. Particle size analysis

Volume-weighted particle size analysis of all individual polymers was conducted using a Sympatec HELOS/RODOS (Clausthal-Zellerfeld, Germany) laser diffraction particle size analyser. The dispersion of air pressure was adjusted to 2.0-bar and a feed rate of 20% was applied. The particle size distributions (PSDs), i.e., particle size at 10% ($D_{10\%}$), 50% ($D_{50\%}$, median diameter), 90% ($D_{90\%}$) of the volume distribution and volume mean diameter (VMD) (mean ± SD, *n* = 3), were all calculated automatically using the WINDOX software based on Fraunhofer theory. Approximately 1 g of each powder was hand-fed into the VIBRI RODOS disperser. A background measurement was taken as the reference test. The measurements were set to trigger when the optical concentration (Copt) was higher than 1.1% and to end when the Copt fell below 1% for 5 s. The time-base was 100 ms and the obstruction was ~ 10-30%.

2.2.2. Powder flow properties

L-HPC powder compressibility was determined by using the Pharma Test (TD1, Hainburg, Germany) mechanical tapping device and following the USP guidelines <616> method I, and ultimately working out each grade's Carr's Index and Hausner ratio. The powder was weighed (50g) and poured into a 250 ml measuring cylinder. The poured volume was recorded. The machine was then set to tap 50 times per test cycle. The tapped volume was recorded, and the machine run again. Tapped volume was again recorded, and the process repeated until a steady tapped volume was obtained. The maximum number of taps delivered per powder was 300. The Carr's Index for each powder was calculated using equation (1):

$$Carr\acute{}s\ Index = \left(\frac{(Dt-Dp)}{Dt}\right) \times 100 \quad [1]$$

The Hausner ratio was also calculated using the equation (2):

$$Hausner\ ratio = \frac{Dt}{Dp} \quad [2]$$

Where Dt is the tapped density and Dp is the poured density.

2.2.3. Scanning Electron Microscopy (SEM)

Zeiss scanning electron microscope (Evo50, Oxford instruments, Inca wave, UK) was used to study the surface morphology and particle size of the four polymers. Fine powder samples were lightly sprinkled on the carbon surfaces of universal specimen stubs and double coated with gold under low vacuum for about 4 min in the presence of Argon gas, using a sputter coater (Polaron SC500, Polaron Equipment, Watford, UK) at 20 mA. The particle surface morphology was captured and analysed using smartSEM software.

2.2.4. Specific surface area analysis

Specific surface area of the four polymers was studied using N_2 adsorption/desorption. Nitrogen adsorption/desorption measurements were carried out at T=77 K with Belsorp-mini (BEL, Japan Inc). The Specific surface area of samples were calculated according to Brunauer-Emmett-Teller (BET) model. Barrett–Joyner–Halenda (BJH) and micropore (MP) methods were used to calculate the pore size distribution of the HPC samples. Before the analysis, samples of about 50-100 mg were degassed undervacuum (about 5 µm Hg) and at T=353 K for 2 h. For the measurement of the samples, a program was used that collects about 50 data points (25 each for adsorption and desorption) evenly distributed between P/P0=0 and P/P0~1.

The specific surface area (as) was calculated using BET graphs and equation 3.

$$a = \frac{V_m}{22414} L\tau \quad [3]$$

Where L is Avogadro constant, V_m is the monolayer volume and t is the cross sectional area of the adsorbate molecule

2.2.5. X-ray powder diffractometry analysis

The main crystalline compounds in the samples were identified by qualitative X-ray powder diffractometry (XRD) using a Siemens D5000 X-ray powder diffractometer with the characteristic copper radiation and a scintillation detector with diffracted intensity of λ = 0.1542 nm at 40 kV and 30 mA) was measured at 2θ ranging between 4° and 50°.

2.2.6. Karl Fisher analysis

Karl Fisher titration was carried out using a KF Automatic titrator (Metrohm 787 Titrino), Aqualine Complete 2 as the KF reagent and anhydrous methanol as the solvent. Samples were opened under a dry environment and dissolved in 3 ml of KF reagent, before re-injection back into the Karl Fischer cell. All measurements were done in triplicate.

2.2.7. Atomic force microscopy study

Atomic force microscopy (AFM) data was collected using a Bruker Dimension Icon® Atomic Force Microscope using QNM PeakForce Tapping® mode at room temperature and ambient humidity. In PeakForce Tapping® mode the probe is oscillating way below its resonance frequency in a sinusoidal motion touching the sample only for a short time and generating the force curve. The data can be analysed separately to obtain information about material properties such as adhesion, modulus or dissipation known as quantitative nanomechanical mapping (QNM). A Probe with 0.4 N/m nominal spring constant and triangular Si3N4 tip was used (Scan Asyst Air, Bruker), with nominal tip radius of 2 nm. The spring constant was calibrated using a thermal-tune method. Deflection sensitivity was calibrated using hard surface (Sapphire, Bruker) Sample immobilized on the metal puck using a double tape. Due to fibrous morphology, small particles size and their random orientation the immobilization of the particles was a significant challenge, hence AFM data were collected from two particles from each sample with scan size of 5 µm, scan rate 1.5 Hz, sample/lines 512. Nanoscope Analysis v1.5 software was used for image analysis. First order plane fit was applied to all height sensor micrographs. Roughness data were obtained from height micrographs using 'Roughness function' in Nanoscope analysis v1.5.

2.2.8. Tablet preparation

In order to evaluate the compressibility and tabletability of L-HPC powders, 500 mg of the powders were accurately weighted out and directly compressed. The powders were directly compressed using a uniaxial hydraulic press (Specac tablet presser, Kent, UK) and 13 mm split, in order to prevent

mechanical failure the decompression process was controlled using . Powders were compressed at compression pressures 74, 148, 22, 295 and 443 MPa, with a dwell time of 30 sec. Cylindrical tablets with diameter of ~13 mm and flat faced surface were obtained. A desiccator containing silicon dioxide was used to maintain relative humidity under 4% (Ebro Data logger, EBI 20-IF, Germany), L-HPC powders and tablets were stored under desiccation for at least 48 hours and at 25 ^{o}C prior to use.

2.2.9. Tablets' porosity measurements

Bulk densities of the prepared tablets were determined by using a digital calliper to measure the dimensions of the pre-weighed tablets. The tablet true density was measured using a helium pycnometer (Multipycnometer Quantachrome Instruments, Hampshire, UK). Both bulk and true density values were used to determine the tablets' porosity using equation 4.

$$\varepsilon = 100(1 - \rho_d / \rho_t) \quad \textbf{[4]}$$

Where ε is the porosity and ρ_d is the bulk density and ρ_t is the true density of the polymer powder. All the measurements were done in triplicate.

2.2.10. Tablet tensile strength measurement

The force required to crush the tablets was measured using a tablet hardness apparatus (Schleuniger 4M, Thun, Switzerland). The measured force was used to determine the tablet tensile strength using equation 5.

$$\sigma = \frac{2F_c}{\pi dt} \quad \textbf{[5]}$$

Where σ is the tablet tensile strength, F_c is the crushing force required to break the tablet, d is the tablet diameter and t is the tablet thickness. All measurements were done in triplicate.

2.2.11. Heckel analysis

The Heckel equation (6) was used to analyse the tablet's compression characteristics.

$$ln\left(\frac{1}{1-D}\right) = KP + A \quad [6]$$

Where D is the tablet relative density at pressure P, K is a material constant (slope of the straight line portion of the Heckel plot) and is 1/3 of the yield strength. The 1/K value is used to express the mean yield pressure and gives an indication of the material's ability to undergo plastic deformation under pressure. A is a function of the initial bulk volume and is calculated from the intercept of the straight line of the Heckel plot. It provides information on the movement/rearrangement of particles at the initial stages of compaction.

2.2.12. Young's/Elastic modulus analysis

The elastic modulus was evaluated using texture profiling analysis (Texture Analyzer, TA.HDplus, Stable Micro Systems, UK). The four polymers were compressed using a 6 mm diameter stainless steel cylindrical flat bottomed probe which was connected to a 750 kgf cell and the powder was compressed using high tolerance powder compaction rig with a compression die of 20 mm height and 6 mm diameter. The samples were compressed to a maximum of 300 kgf with the probe moving at test speed of 2 mm/s. A correlation between the stress (MPa) and strain (%) was established and the Texture Exponent software was used to work out the gradient of the initial linear part of the graph.

2.2.13. Disintegration time studies

In vitro disintegration time was evaluated using the US pharmacopoeia (35) monograph (<701> disintegration). An Erweka ZT3, GMBH (Heusenstamm, Germany) was used in this study as the disintegration apparatus and distilled water (800 ml) as the disintegration medium. The temperature was thermostatically maintained at 37 °C. Three tablets were placed in the basket rack assembly and covered with a transparent plastic disk. The disintegration time was taken as the time required for tablets to disintegrate completely without leaving any bulk solid residue. All the measurements were carried out in triplicate and presented as mean ± standard deviation.

2.2.14. Statistical analysis

All formulations were prepared and analysed in triplicate and the results were expressed as mean± standard deviation. Minitab® (version 17.1.0) was used to statistically evaluate the date obtained; the results were analysed using Mann-Whitney test.

Results and discussion

2.3. Powder flowability

Powder flow plays a crucial role in the numerous processes of pharmaceutical manufacturing, including pellet, granules and tablet formation and capsule filling. Hence, good flowability is required to ensure uniform and consistent feed from bulk storage containers into the feeder during the manufacturing process. Looking at the tabletting process, a good flowability ensures uniformity of the tablets' contents. The flowability of the four HPC powders was assessed using the Hausner ratio and Carr's index. LH32 showed the highest flowability with a Carr's index of 7.83, while LHB1 had poor flow properties with a Carr's index of 28.6 (Figure 2a).

2.3.1 Particle size analysis

In order to understand the flowability behaviour of L-HPC powders, the particle size of the four powders was assessed using laser diffraction. Particle size analysis for the four grades of L-HPC is summarized in figure (2b). The data showed that low substituted hydroxyl propyl cellulose of LH32 grade has the lowest particle size with a volume mean diameter of 31.36±0.08 µm. On the other hand, all the other grades showed larger particle sizes with volume mean diameters between 55.12±0.09 to 59.45±0.09 µm. The study of the flow properties of the four powders, showed LH32 to have the best flow properties, despite having the smallest particle size amongst all HPC grades. Moreover, both LH21, LH11 showed different flow behaviour compared to LHB1 particles despite sharing the same volume mean diameter. Particle size is not the only determinant of the flow properties of pharmaceutical powders; the shape of the powder also plays an important role in the powder flowability. Therefore, the morphology of the four grades was evaluated using SEM.

2.3.2. Scanning Electron Microscopy

SEM images showed that the majority of LH32 particles were small and circular in shape, with a diameter of around 20 µm (Figure 3a). LH32 circular particles were mixed together with a small population of long fibres and both had a rough solid surface. On the contrary, LH21 and LH11 powders, (Figures 3b and 3c respectively) were dominated by long fibres. Fibrous particles have high aspect ratios, which are associated with higher static and dynamic friction, which in turn reduces the mass flow and powder flowability as suggested by (Horio et al., 2014). This could explain the poor flow properties of LH11 and LH21 as both samples were dominated by fibrous particles with high aspect ratios. On the other hand, looking at the LHB1 particles under the microscope showed that

the sample was dominated by spherical particles with diameters of around 50 µm (Figure 3d). Because of the high population of spherical particles with low aspect ratios and large particle size, it was expected that LHB1 would have superior flow properties. Nonetheless, the flow data showed a different trend. As reflected by the SEM results, the four polymers contained mixtures of circular and fibrous particles and this explains the wide range of particle size distribution to represent the smallest minor diameter to the largest major diameter of the L-HPC powders.

2.3.3. Moisture Content Analysis

The powder flow is affected primarily by two forces; friction and cohesion (Nokhodchi, 2005). In addition to the particles' shape and size, moisture content will affect the friction and cohesion forces. For instance, high moisture content in pharmaceutical powders will increase the frictional forces, by increasing the static coefficient of friction between the particles (Karimi et al., 2009). , Moisture, however, diminishes the effect of electrostatic charges between particles, and in addition the water content generates solid bridges between particles. This increases the cohesion forces and thus affects the powder flow (Amidon and Houghton, 1995). The moisture content of the four powders was assessed using Karl Fisher analysis (Table 2). LH-32 showed the highest moisture content of 3.02±0.27 ($P<0.1$), followed by LHB1 (2.52±0.17), then LH21 and LH11 (Table 2). In general, moisture content is inversely proportional to the powder flow rate i.e. increasing the moisture content of the powder will be associated with a decrease in the flow rate which means a decrease in powder flowability (Crouter and Briens., 2014). The effect of adsorbed moisture on powder behaviour becomes pronounced at moisture levels greater than 5%, as water acts as a plasticizer and reduces the glass transition of the polymers, as seen in case of microcrystalline cellulose (Sun C., 2007). All HPC powders showed low moisture content, which suggested that the flow behaviour of these powders could not be explained on this basis. It could be concluded that the LH21 and LH11 poor flow properties were attributed to the morphology of their particles. Their fibrous structure and high aspect ratios reduced the flow properties. On the other hand, the particles' morphology, size and moisture content analysis failed to explain the flow behaviour of LH32 and LHB1.

2.4. Powders compressibility profiles

The densification properties of the four L-HPC powders were studied by evaluating the changes in the powders' porosity at various compression pressures. Materials with superior compression profiles are able to respond to high compression pressure by reducing their porosity, which could play a role in increasing the contact surface area between particles, and enhance increasing particles binding. Generally increasing the compression pressure was associated with decreasing the tablets' porosity (Fig 4). LHB1 showed the highest compressibility profile with a porosity of (0.61±0.011) at a compression pressure of 74 MPa ($P<0.1$), which reduced by around 0.10 at 295 MPa. This was followed by LH21, LH32 then LH11. LH32 powders changed their porosity by 0.08 when increasing the compression pressure by 369 MPa (i.e between 74 and 443 MPa).

*Table 2: Summary of moisture content (%), yield pressure (MPa), yield strength and tensile strength at f σ0 or LH32, LH21, LH11 and LHB1, * (P<0.1).*

Polymer grade	Powder true density	Moisture content (%)	Yield Pressure (MPa) 1/k	Yield strength	Tensile strength at zero	Young's Modulus (MPa)

	(g/cm^3)				porosity (σ_0)	
LH32	2.67±0.04*	3.02±0.27*	2000	666.66	108.68	0.08±0.01*
LH11	2.57±0.04*	2.32±0.16	625	208.33	9171.50	0.37±0.02*
LH21	2.55±0.02*	2.32±0.18	434.78	144.92	1120.30	0.21±0.05*
LHB1	2.78±0.02*	2.52±0.17	769.23	256.41	5081.40	0.64±0.11*

Table (2) summarizes the yield strength and yield pressure of the four powders. The Heckel analysis (Figure 4) revealed that LH21 powder had the highest plasticity amongst the four L-HPC grades, followed by LH11 and LHB1.

The stress/strain profiles revealed that LH32 powder has elastic properties and is more flexible than the rest of the powders as reflected by its low Young's modulus (0.08±0.01) Table (2). This means that LH32 tends to reversibly deform and change its shape considerably under mechanical loading. Besides, LH32 showed a high yield pressure of (2000 MPa), which suggests the need of high compression pressure to permanently deform the material to move from the elastic region to the plastic region of LH32 for an irreversible deformation. Moreover, pharmaceutical materials with high elastic region yield strength are typically associated with manufacturing complications such as capping, lamination and tablet breakage. This suggests that some issues could be associated with compressing LH32 powder.

The formation of strong compacts during densification also known as compactability was studied for the four L-HPC grades. Figure (6) shows that the tensile strength of LH11 and LHB1 decreases exponentially decrease with increasing of porosity. All the four polymers showed a strong exponential correlation with correlation coefficient ranging between 0.94 and 0.96. The compactability profile of each powder was evaluated by calculating the tensile strength at zero porosity (σ0) using the Ryshkewitch equation. σ0 was found to be 9171.50 MPa and 5081.40 MPa for LH11 and LHB1 respectively. The high σ0 of LH11 and LHB1 suggested strong bond formation between particles during the densification of the polymers' powders. The formation of a compact or tablet of a specific strength under compaction pressure is known as tabletability. Both compressibility and compactabiltiy play a role in the tabletability. Powders with high compressibility possess lower porosity under compression and are expected to have a higher inter-particulate bonding area. While high compactability reflects the ability of the powder to form strong bonds under compression. Both the large surface area and strong bond formation are necessary form good tabletability. Figure (7) shows the tabletability profile of the four polymers. LH32 showed the highest tensile strength at all compression pressures. The polymer had a tensile strength of 5.21 MPa at 74 MPa that increased to 8.32 MPa at 443 MPa. Nonetheless, the tensile strength remained steady

between 148 and 295 MPa. This could be attributed to the poor compressibility of LH32, as demonstrated in Figure (5). On the other hand, LHB1 showed the lowest tabletability profile with a mean tensile strength of 0.81 at 74 which steadily increased to 3.00 MPa at the maximum applied compression pressure. LH32 tabletability was high despite having a weaker compressibility and poorer plastic properties. The poor tabletability of LHB1 could be associated with a failure in the bond formation of the polymer's particles. In order to have a better understanding of the behaviour of LH32 and LHB1, specific surface area analysis was conducted using the Brunauer-Emmett-Teller method. Nitrogen adsorption and desorption isotherms and t-plots are summarized in Figure (8 a&b). All the four polymers showed adsorption/desorption isotherms of type III, revealing a weak interaction between the L-HPC polymers and the adsorbate; moreover, type III isotherms reflect the nonporous structure of the polymers. BET analysis showed that LH32 had the largest pore volume ($1.4x10^{-2}$ cm^3) and the highest specific surface area (1.47 m^2/g). The high surface area could be attributed to the high content of small particles in the LH32 sample as suggested by the SEM images. On the other hand, LHB1 had the lowest specific surface area of (0.24 m^2/g). The high tabletability behaviour of LH32 could be attributed to the high specific surface area as suggested earlier by Paluch et al (Paluch et al., 2013). Paluch and co-workers concluded that a materials' specific surface area had a direct impact on powders' tabletability, as it was observed that materials with large specific surface area could compact well even at low compression pressure. A similar trend was observed for LH32, with its tablets having a tensile strength of 5.21 MPa at 74 MPa compared to a tensile strength of 0.81 MPa for LHB1 at the same compression pressure. Fibrous samples such as LH21 and LH11 showed lower specific surface areas of 0.84 and 0.91 respectively.

Moisture content of pharmaceutical samples is another factor that is believed to play a significant role in powder compaction, as water exhibits plasticizing effects (Sun 2008; Nokhodchi 2005). In this study, the effect of moisture would be minimal as the moisture content was low and the difference between LH21, LH11 and LHB1 polymers was insignificant (P>0.1) (Table 2). On the other hand, LH32 had a significantly higher moisture content of 3.02±0.27 compared to LH11 and LH21 (P>0.1) and this might have played a role in increasing the tabletability of LH32.

Table 3: BET (Brunauer-Emmett-Teller) surface area, Mean pore diameter, $^{\#}$Total pore volume at relative pressure (P/P_0 = 0.97). *P<0.1.

Material	BET specific surface area (m^2/g)	t plot total specific area (m^2/g)	Total pore volume$^{\#}$ (cm^3)	Roughness (nm)	Adhesion force nN)
LH32	1.47	1.5	$1.4x10^{-2}$	100.09±18.84	5.91 ± 1.63
LH11	0.91	0.87	$6.08x10^{-3}$	2.43±1.41 *	9.50±5.78
LH21	0.84	0.85	$5.5x10^{-3}$	9.07±14.42 *	21.01±11.35
LHB1	0.24	0.24	$7.8x10^{-3}$	21.18±13.19	5.33 ± 3.61

It is also believed that crystal structure and orientation within pharmaceutical powder will have an impact on the macroscopic properties of the material. X-ray diffraction of the L-HPC polymers was investigated and data is summarised in Figure (9). XRD analysis did not reveal any sharp reflections and all the L-HPC samples exhibited a large diffuse halo at 2Θ between 15^{o} -25^{o}. This halo reflected the amorphous features of the four L-HPC grades and is believed to play a role in the swallowing behaviour of HPC polymers (Yamamoto et al. 2010; Palmeiro-Roldán et al., 2014). Because of the similarity in the XRD profiles, it was strongly believed that the crystal structure of L-HPC polymers had no effect on their compaction behaviour.

Surface roughness (R_a) is another factor that could be of particular importance in tablet formation as it was reported that surface roughness affected the contact area between particles depending on the size and distribution of asperities on the surface (Cooper et al., 2001; Beach et al., 2002). Atomic force microscopy (AFM) can provide useful information about particles properties such as perimeter, height and surface roughness, by providing a three-dimensional image at a vertical resolution of sub-nanometer scale and lateral resolution of a few nanometers (Figures 11).

AFM data showed that LH32 particles had the highest surface roughness of 100.09±18.84 nm ($P< 0.1$ compared to LHB1). The high surface roughness could also explain the large specific surface area of LH32 as revealed by BET studies and reported previously by Katsikogianni and Missirlis and Anitha et al (Katsikogianni and Missirlis; Anitha et al., 2016). Nonetheless, increasing surface roughness is associated with lower contact area, as the particles will contact at the tips only (Figure 12), hence the low adhesion forces between LH32 particles (5.91 ± 1.63 nN). The AFM data revealed that decreasing the surface roughness was associated with an increase in the adhesion forces (Figure 11), which came in line with Cheng et al's (Cheng et al, 2002) studies. In particular, particles with smoother surfaces would have a larger area of contact with one another and higher chances of bond formation, hence stronger adhesion forces. LH32 particles have large surface roughness and it is believed that LH32 particles bind through mechanical interlocking and this could explain the superior tensile strength of LH32 powder as suggested by Moon and Jang (Moon and Jang, 1999). On the other hand, LH21 particles showed strong adhesion forces between particles (21.01± 11.35 nN), which came in line with Heckel's analysis, suggesting that LH21 powder compacted by plastic deformation. A similar trend was observed for LH11, which exhibited an adhesion force of 9.50±5.78 nN.

Disintegration studies of the compacted tablets were evaluated and summarized in Figure (13). LHB1 tablets disintegrated within 150.67±4.04 s at low compression pressure and the disintegration time increased to 573.67±20.3 s at 443 MPa ($P< 0.1$ vs LH32). On the other hand, LH32 tablets only managed to disintegrate at 74 MPa and failed to break down when the compression pressure increased above 74 MPa. This could be attributed to the low porosity of LH32 tablets as reported earlier under the compressibility section. LH32 tablets had a porosity of 0.22±0.01 at 74 MPa which dropped further upon increasing the compression pressure. The low porosity hindered water

permeation across the tablets and delayed the disintegration. Similar trends were observed in studies carried out by Alvarez-Lorenzo (Alvarez-Lorenzo, 2000). Moreover, it had been reported that the swelling rate and swelling work (swelling force) and the speed of water penetration affected the rate of tablet disintegration. Upon swelling of the polymer a pressure was generated resulting in disintegration of the tablets. Kawashima et al (Kawashima et al, 1993) reported that the swelling rate and swelling work were affected by the particle size of L-HPC polymers. Studies showed that fine particles had less ability to uptake water and did not swell as quickly as HPC polymers with large particle size. LHB1 was reported to reach 100% swelling within less than 50 seconds followed by LH11, LH21, then polymers with fine particles such as LH31 (Shin-Etsu). This explained the fast disintegration of LHB1 tablets and the long disintegration time for LH32, which had a mean volume diameter of 31.36±0.08 μm. Besides, the content of hydroxypropoxy (HPO) was believed to play a role in the swelling abilities of L-HPC polymers, as L-HPC polymers with low HPO content such as LH32 swell less than polymers with high HPO content.

3. Conclusion

The macro and micrometric properties of L-HPC polymers affect their compaction and disintegration behaviour. LH32 powder showed a large specific surface area due to its small particle size and rough surface. Nonetheless, under compression the polymer is believed to compress by mechanical interlocking rather than plastic deformation, as the rough surface of the LH32 powder mediates and enhances the mechanical interlocking during compression. On the other hand, L-HPC polymers with smooth surfaces such as LH21 and LH11 are believed to have larger areas of contact, which enhances adhesion. Together with the small elastic region, LH21 and LH11 compress via plastic deformation. Among the four powders, only LHB1 demonstrated superior disintegration behaviour and can be successfully used in preparing ODTs with both good mechanical strength and fast disintegration time.

References

Alvarez-Lorenzo C, Go´mez-Amoza JL, Martı´nez-Pacheco R, Souto C, Concheiro A. 2000. Evaluation of low-substituted hydroxypropylcelluloses (L-HPCs) as filler-binders for direct compression. International Journal of Pharmaceutics. 197: 107–116

Amidon GE, Houghton, ME. 1995. The effect of moisture on the mechanical and powder flow properties of microcrystalline cellulose. Pharm. Res. 12: 923–929.

Anitha VC, Hamnabard N, Banerjee A, Dillip, GR, Joo SW. 2016. Enhanced electrochemical performance of morphology-controlled titania-reduced graphene oxide nanostructures fabricated via a combined anodization-hydrothermal process. RSC Adv. 6: 12571.

Azizi Samir, MAS, AlloinF, Dufresne A. 2005. Review of recent research into cellulosic whiskers, their properties and their application in nanocomposite field. Biomacromolecule. 6: 612–26.

Beach E R, Tormoen GW, Drelich J, Han R. 2002. Pull-off Force Measurements between Rough Surfaces by Atomic Force Microscopy., Journal of Colloid and Interface Science. 247: 84–99

Cheng W, Dunn PF, Brach RM. 2002. Surface roughness effects on microparticle adhesion. The Journal of Adhesion. 78: 929–965.

Cooper K, Gupta A, Beaudoin S. 2001. Simulation of the Adhesion of Particles to Surfaces., Journal of Colloid and Interface Science. 234: 284–292.

Crouter A, Briens L. 2014. The Effect of Moisture on the Flowability of Pharmaceutical Excipients. AAPS PharmSciTech. 15: 1.

Diós P, Pernecker T, Nagy S, Pál S, Dévay A. 2015. Influence of different types of low substituted hydroxypropyl cellulose on tableting, disintegration, and floating behaviour of floating drug delivery systems., Saudi Pharmaceutical Journal. 23: (6), 658–666.

Fox SC, Li B, Xu D, Edgar KJ. 2011. Regioselective Esterification and Etherification of Cellulose: A Review Biomacromolecules. 12: (6), 1956-72.

Hebeish A, Guthrie J T. 1981. The Chemistry and Technology of Cellulosic Copolymers, Springer-Verlag, Berlin.

Horio T, Yasuda M, Matsusaka S. 2014. Effect of particle shape on powder flowability of microcrystalline cellulose as determined using the vibration shear tube method. Int J Pharm. 473: (1-2):572-8

Ishikawa T, Mukai B, Shiraishi S, Utoguchi N, Fuji M, Matsumoto M, Watababe Y. 2001. Preparation of rapidly disintegrating tablet using new types of microcrystalline cellulose (PH-M series) and low substituted-hydroxypropylcellulose or spherical sugar granules by direct compression method. Chem Pharm Bull (Tokyo). 49: (2), 134-139.

Karimi M, Kheiralipour K, Tabatabaeefar A, Khoubakht GM, Naderi M and Heidarbeigi K. 2009. The Effect of Moisture Content on Physical Properties of Wheat. Pakistan Journal of Nutrition. 8 (1): 90-95.

Katsikogianni M, Missirlis YF. 2004. Concise review of mechanism of bacterial adhesion to biomaterials and techniques used in estimating bacteriamaterial interactions. Eur. Cells Mater. 8: 37–57

Kawashima Y, Takeuchi H, Hino T, Niwa T, Lin T, Sekigawa F, Kawahara K. 1993. Low-Substituted Hydroxypropylcellulose as a Sustained-Drug Release Matrix Base or Disintegrant Depending on Its Particle Size and Loading in Formulation. Pharmaceutical Research. 10: (3), 351-355.

Klemm B, Heublein HP, Bohn A. 2005. Angew. Chem., Int. Ed. 44, 3358–3393.

Kojima M, Nakagami H. 2002. Investigation of Water Mobility and Diffusivity in Hydrating Micronized Low-substituted Hydroxypropyl Cellulose, Hydroxypropylmethyl Cellulose, and Hydroxypropyl Cellulose Matrix Tablets by Magnetic Resonance Imaging (MRI)., Chemical and Pharmaceutical Bulletin. 50: (12), 1621-1624.

Moon S I, Jang J. 1999. The mechanical interlocking and wetting at the interface between argon plasma treated UHMPE fiber and vinylester resin. Journal of materials Science. 34: 4219 – 4224

Nokhodchi A. 2005. An overview of the effect of moisture on compaction and compression. Pharm. Technol. 46–66.

Ogawa A, Nakayama S, Uehara M, Mori Y, Takahashic M, Aibab T, Kurosakia Y. 2014. Pharmaceutical properties of a low-substituted hydroxypropyl cellulose (L-HPC) hydrogel as a novel external dressing. International Journal of Pharmaceutics. 477: (1–2), 546–552

Onda Y, Muto H, Suzuki H. 1978. Method for preparing low-substituted cellulose ethers. Publication number US4091205 A, 23.

Palmeiro-Roldán R, Fonseca-Berzal C, Gómez-Barrio A, Arán VJ, Escario J, Torrado-Durán S, Torrado-Santiago S. 2014. Development of novel benznidazole formulations: Physicochemical characterization and in vivo evaluation on parasitemia reduction in Chagas disease., International Journal of Pharmaceutics. 472: 110–117

Paluch KJ, Tajber LOI, Healy AM. 2013. Impact of Alternative Solid State Forms and Specific Surface Area of High-Dose, Hydrophilic Active Pharmaceutical Ingredients on Tabletability., Mol. Pharmaceutics. 10: 3628−3639

Purves CB. 1946. Chemical nature of cellulose and its derivatives. InterScience, NewYork.

Roy D, Semsarilar M, Guthrie JT, Perrier S. 2009. Cellulose modification by polymer grafting: a review. Chem. Soc. Rev., 38: 2046-2064.

Shin-Etsu http://www.elementoorganika.ru/files/lhpc.pdf (Accessed 20/08/2016)

Shirai Y, Sogo K, Fujioka H, Nakamura Y. 1994. Role of low-substituted hydroxypropylcellulose in dissolution and bioavailability of novel fine granule system for masking bitter taste., Biol. Pharm. Bull. 17: 427–431

Sunada H, Bi Y. 2002. Preparation, evaluation and optimization of rapidly disintegrating tablets. Powder Technology. 122: (2-3), 190-193.

Sun C. 2007. Mechanism of moisture induced variations in true density and compaction properties of microcrystalline cellulose. Int J Pharm. 346: 93–101

Sun CC. 2008. Mechanism of moisture induced variations in true density and compaction properties of microcrystalline cellulose., International Journal of Pharmaceutics 346: 93–101

Torre-Iglesias PM, García-Rodriguez J, Torrado G, Torrado S, Santiago S, Bolás-Fernández F. 2014. Enhanced bioavailability and anthelmintic efficacy of mebendazole in redispersible microparticles with low-substituted hydroxypropylcellulose. Drug Des Devel Ther. 8: 1467–1479.

Yamamoto E, Kiyose M, Yamane C, Midorikawa T, Takahashi T, Ishihara M, Mori M. 2010. Structure and Properties of L-HPC(Low-Substituted Hydroxypropyl Cellulose) Films and Fibers Regenerated from Aqueous Sodium-Hydroxide Solution. Polymer Preprints Japan. 53: (2).

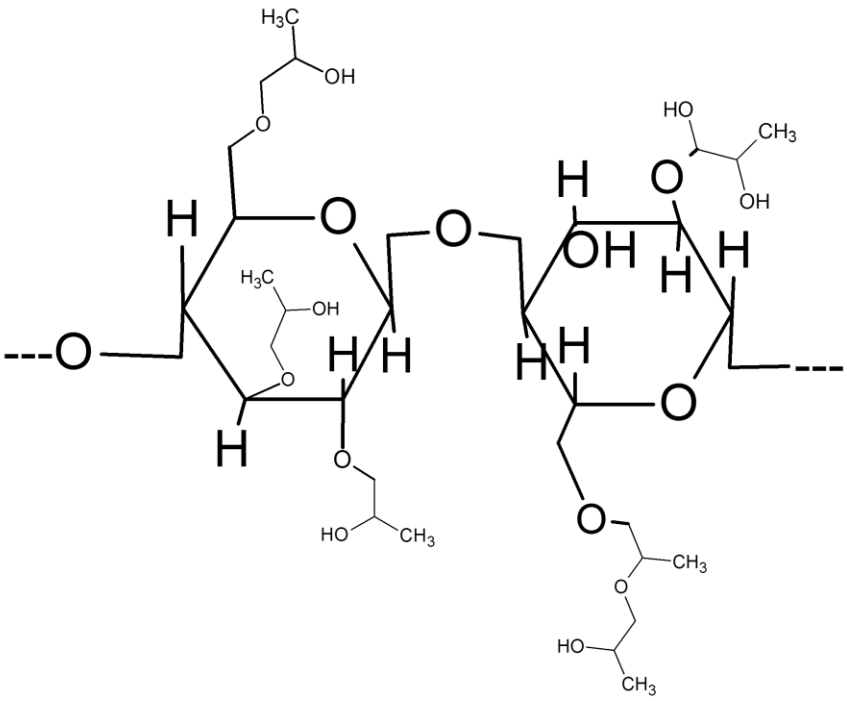

Figure 1: Chemical structure of hydroxypropylcellulose

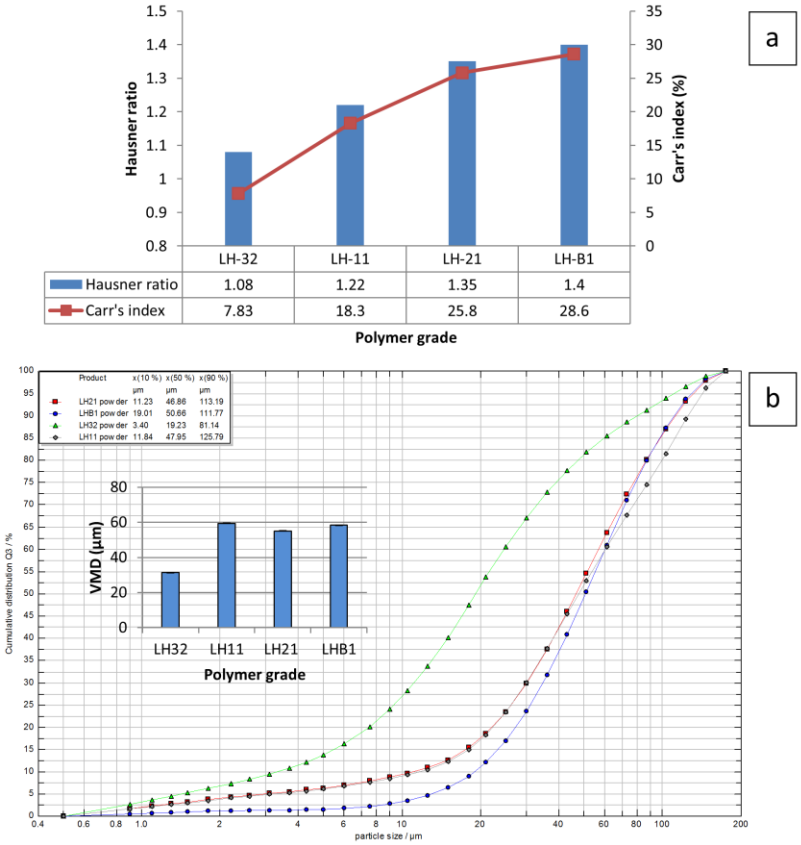

Figure 2: Hausner ratio and Carr's index of the LH32, LH21, LH11 and LHB1 polymers (a) and laser diffraction particle size analysis using (b).

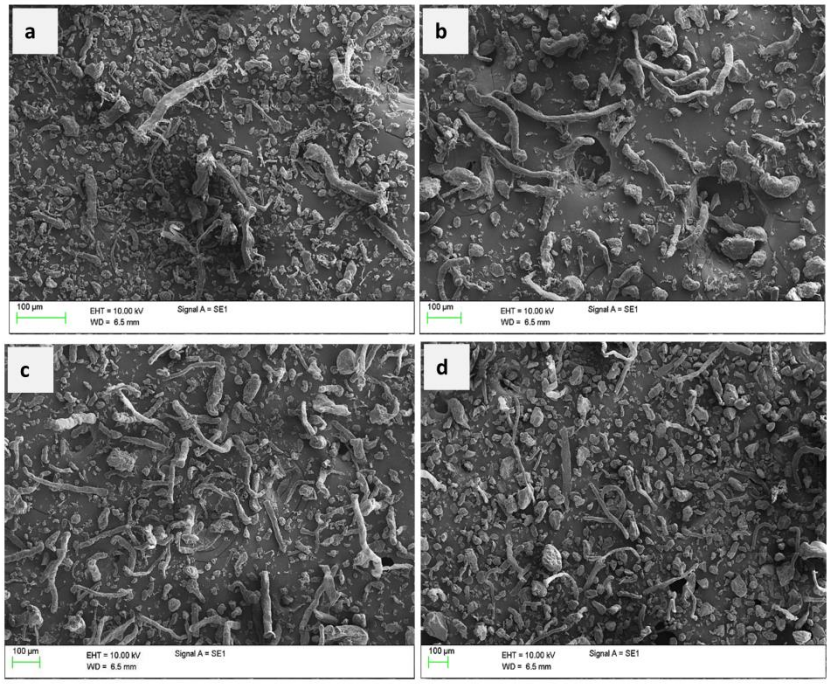

Figure 3: SEM images of LH32 (a), LH21 (b), LH11 (c) and LHB1 (d)

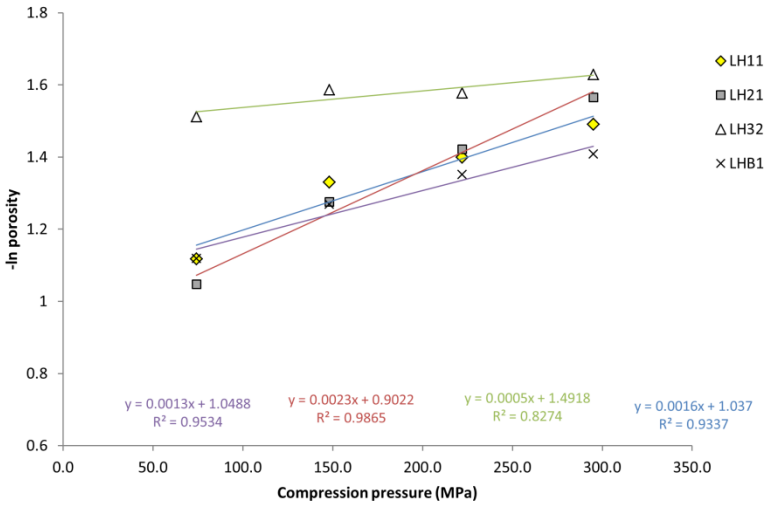

Figure 4:- Heckel plot showing the correlation between – lnporosity and the compaction pressure (MPa) for LH11, LH21. LH32 and LHB1.

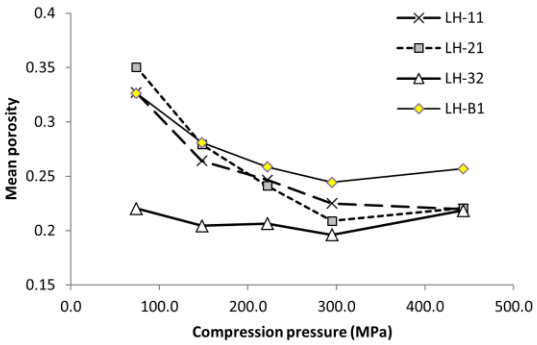

Figure 5: Compressibility profiles showing the correlation between mean porosity of LH32, LH21, LH11 and LHB1 tablets at various compression pressures.

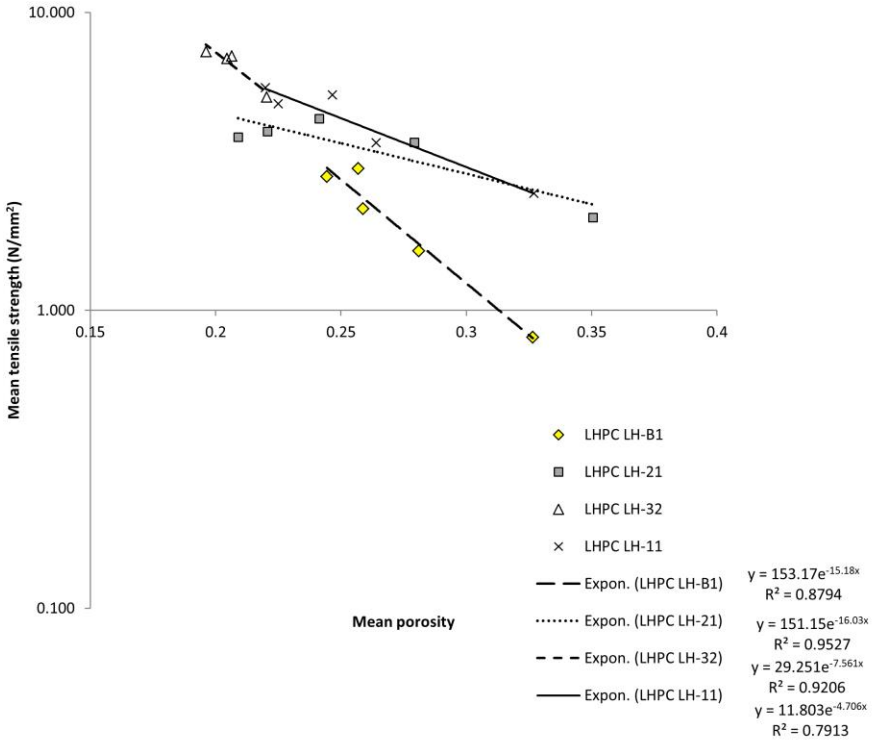

Figure 6: Compactability profiles showing the correlation between mean tensile strength (N/mm2) of LH32, LH21, LH11 and LHB1 tablets at various porosities.

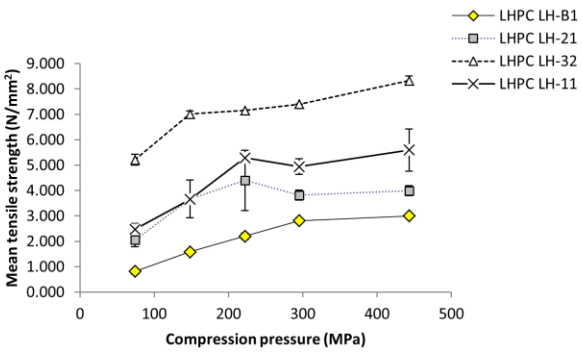

Figure 7:- Tabilitability profiles showing the correlation between mean tensile strength (N/mm2) of LH32, LH21, LH11 and LHB1 tablets at various compression pressure.

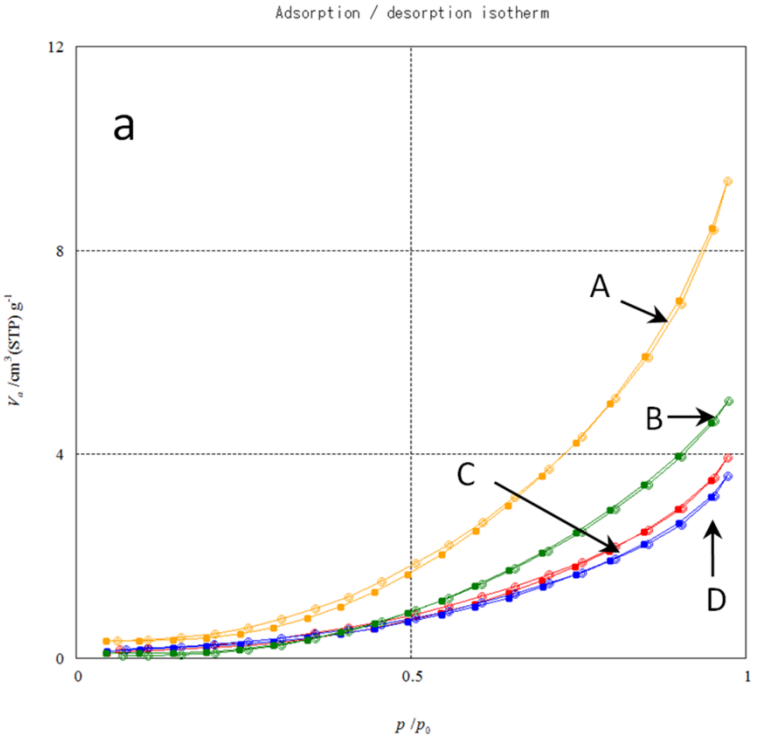
Adsorption / desorption isotherm
a
A
B
C
D
12
8
4
0
0
0.5
1
V_a /cm^3(STP) g^{-1}
p /p_0

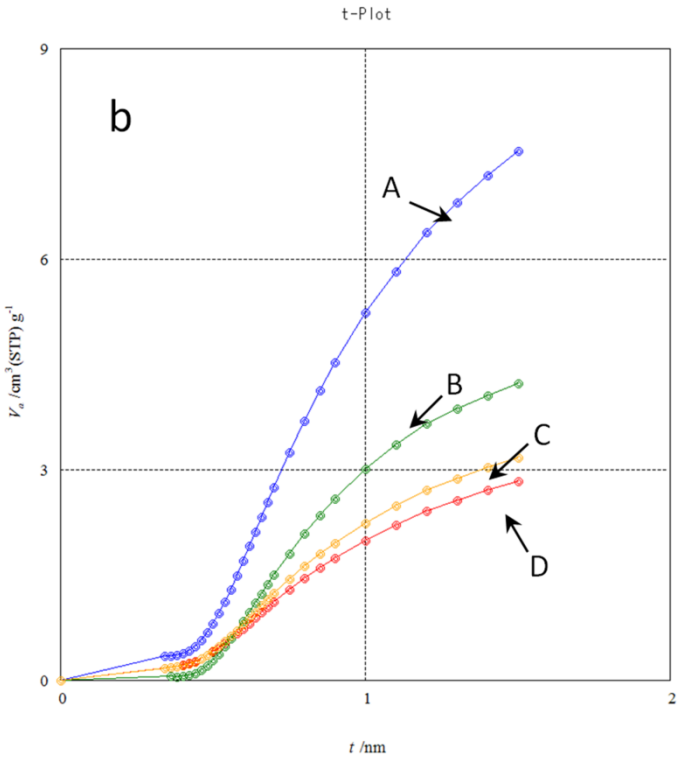
t-Plot
b
A
B
C
D
9
6
3
0
0
1
2
V_a /cm^3(STP) g^{-1}
t /nm

Figure 8: showing the adsorption/desorption isotherm (a) and t-plot (b) for LH32 (A), LHB1 (B), LH11 (C), LH21 (D) where Va is the specific amount adsorbed expressed in the gas volume at standard state (STP T=273.15 K, 101.3 kPa) on 1 g of sample, P/P0 is the relative pressure and t is the adsorption layer thickness.

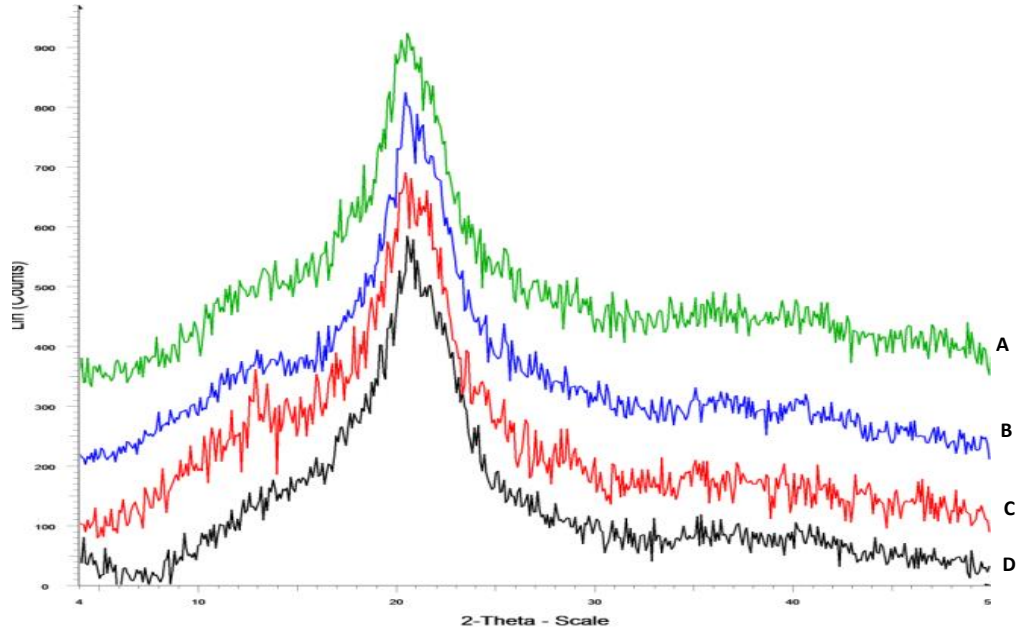

Figure 9: XRD diffraction pattern for LHB1 (A), LH32 (B), LH21 (C), LH11(D)

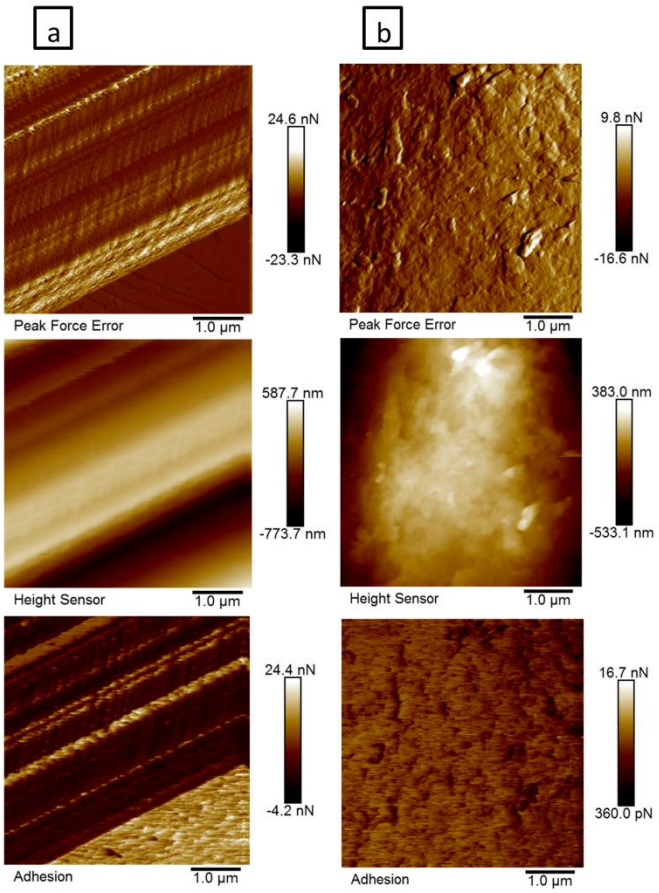

Figure 10: Peak force error, height micrograph and adhesion maps for LH11 (a), LHB1 (b). LH21 (c), LH32 (d).

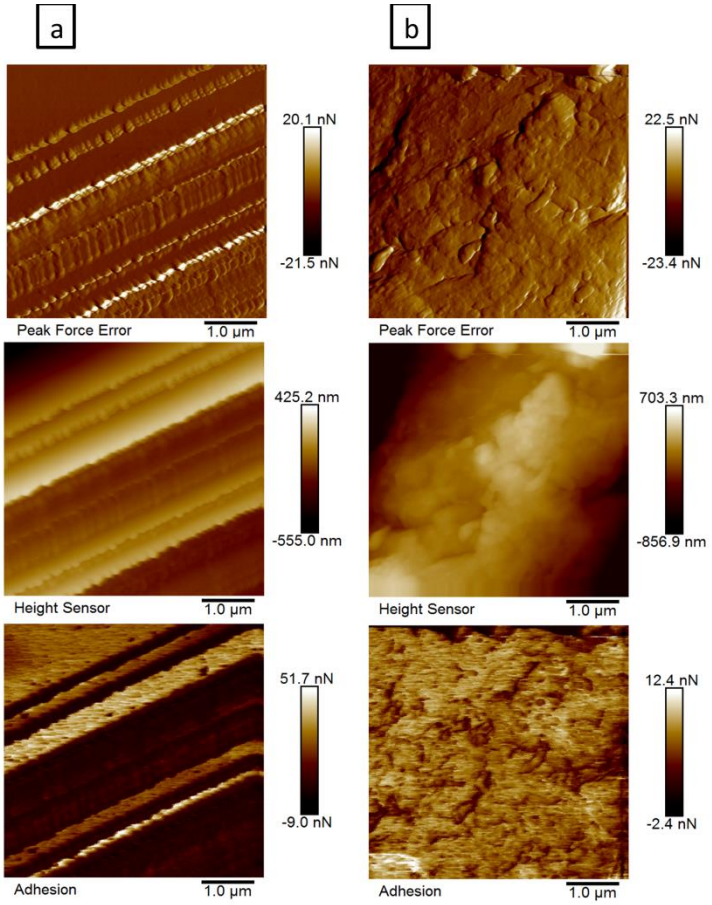

Figure 11: Peak force error, height micrograph and adhesion maps for LH21 (a), LH32 (b).

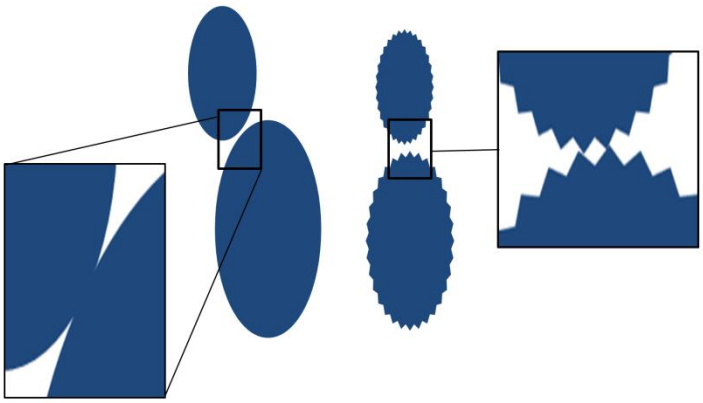

Figure 12: Schematic presentation demonstrating the effect of surface roughness on the contact surface area.

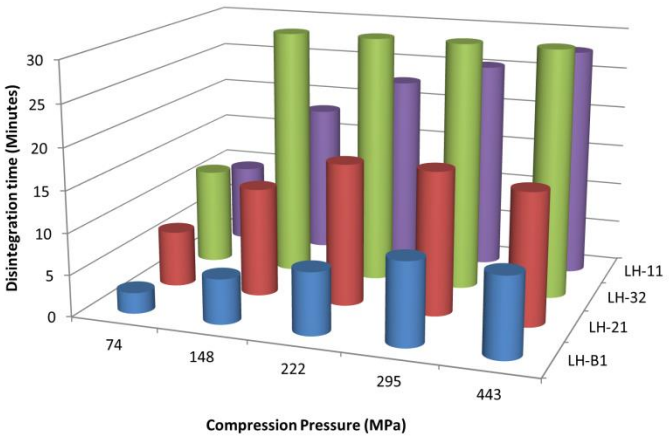

Figure 13: Disintegration times in seconds for LH32, LH21, LH11 and LHB1 tablets.